Synthesis and Application of Modified Orchard Waste Biochar for Efficient Scavenging of Copper from Aqueous Solutions

Abid Hussain[1] · Ubaida Yousaf[1,5] · Usama Rahman Ch[1,5] · Jahangir Ahmad[1,2] · Mohsin Nawaz[3] · Hafiz Nazar Faried[4] · Tanveer Ul-Haq[1]

Abstract

Efficient adsorbents were fabricated by modifying the orchard waste biochar (BC) to produce zero-valent iron composited BC (BC/Fe^0) and phosphorus embedded BC (BC/P). The efficacy of these adsorbents for copper [Cu(II)] removal from aqueous media was investigated via pH, kinetics, and adsorption batch trials. The solution pH 7 was found optimum for the highest Cu(II) removal. Elovich model was fitted well to the Cu(II) kinetics adsorption and higher initial sorption rate 79.44, 75.71, 72.28, 61.60 mg g^{-1} min^{-1} for BC/Fe^0, BC, AC, and BC/P, respectively, was observed than other kinetic models. Langmuir, Freundlich, and Redlich–Peterson isotherm models were applied to the experimental data and Langmuir model fitted well predicting the adsorption capacity of 427.11 mg g^{-1}. The BC became more selective in copper removal after the introduction of Fe^0, and a higher removal rate of Cu(II) was observed in a short time compared to the other tested adsorbents. Therefore, zero-valent iron composited orchard waste-derived biochar as a green and cost-effective adsorbent can open new ways for the efficient removal of Cu(II) from aqueous solutions.

Keyword Adsorption · Biochar composites · Heavy metals · Isotherms · Kinetics modelling · Removal mechanism

1 Introduction

The metals/metalloids are the primary class of inorganic pollutants worldwide. The release of these metals/metalloids from industries due to the ever-increasing population causes devastating environmental damages resulting in severe health concerns. Around two hundred million people die each year worldwide due to water-borne diseases and non-fatal disorder [1, 2]. Due to the increased population, pressure on industries is increasing and these industries are draining a lot of waste containing heavy metals. Waste from agriculture, industries, domestic, and municipality is polluting the world's water as well as decreasing its quality drastically. The industrial and domestic wastewater is the main contributor to the increased concentration of metals/metalloids in sewage sludge. The metals/metalloids in water like copper (Cu), cadmium (Cd), zinc (Zn), and lead (Pb) are ubiquitous and detrimental to flora, fauna, and human when exceeding permissible limits [3, 4]. Heavy metals are toxic even in minute concentrations [5, 6]. These metals/metalloid ions cause serious health problems for human beings, plants, and animals when entering into their food chain [7]. In peri-urban areas, metals/metalloids such as copper [Cu(II)] may enter the food chain through irrigation water as a contaminant.

Copper is a standard metal found innately in the environment and disseminates through industrial and anthropogenic activities such as smelting, mining, electroplating, brass manufacturing, petroleum refining, and agrochemicals [2, 8]. The wastewater produced from these industries

✉ Abid Hussain
abid.hussain@mnsuam.edu.pk

[1] Department of Soil and Environmental Sciences, Muhammad Nawaz Shareef University of Agriculture Multan, Multan 66000, Pakistan

[2] Soil Sciences Department, College of Food and Agricultural Sciences, King Saud University Riyadh Kingdom of Saudi Arabia, Riyadh, Saudi Arabia

[3] Department of Agricultural Engineering, Muhammad Nawaz Shareef University of Agriculture Multan, Multan 66000, Pakistan

[4] Department of Horticulture, Muhammad Nawaz Shareef University of Agriculture, Multan, Multan 66000, Pakistan

[5] Faculty of Bioscience Engineering, Universiteit Gent, 9000 Gent, Belgium

contains a high concentration of Cu(II) and triggers water quality issues [9]. When a considerable amount of Cu(II) is inhaled or consumed, it can accumulate in the liver and causes gastrointestinal and respiratory disorders [10]. Cu(II) ingestion can also cause kidney damage, stomach disorder, anaemia, and sometimes coma leading to death [11]. In microorganisms, Cu(II) causes plasma membrane disruption. The consumption of polluted water for a more extended period causes cancer and results in kidney and reproductive system disorders [12, 13]. The effects of chemicals contamination on human health are chronic [14]. Therefore, there is a dire need to assess the impact of polluted water on human health to avoid severe health problems, which is still a significant cause of the increased mortality rate in many developing countries. To avoid serious consequences, it is needed to treat water before being consumed [15, 16].

The removal of metals/metalloids from potable water is a real challenge because of their complex formation with naturally occurring organic matter [17, 18]. Many techniques, including reverse osmosis, chemical precipitation, ion exchange, filtration, electrodeposition, ultra-filtration, solvent extraction, and adsorption, have been used to remove metals/metalloids from wastewater [15]. Every technique has its pros and cons; however, adsorption is found as an efficient technique to remove Cu(II) from the polluted water [8]. Many adsorbents have been reviewed for the removal of Cu(II), such as granular and powder activated carbon, manganese oxide-coated sand, grafted silica, electric furnace slag, water treatment sludge, aluminium oxides, zeolite, carbon nanotubes, vanillin chitosan membrane, kaolinite, and montmorillonite [19, 20]. However, less attention has been given to convert the orchard waste into valuable adsorbent material to treat the contaminated water metals/metalloids. Thus, we proposed converting orchard waste into biochar to produce an efficient adsorbent for Cu(II) removal from water.

Biochar is a black coloured carbonaceous solid, which has gained popularity as an efficient adsorbent to remove environmental pollutants. [6, 21]. It contains useful functional groups, a large surface area, and high porosity. [22–24]. However, heterogeneity in the biochar structure affects the performance of biochar. In this study, biochar modification was carried out with foreign material, such as zero-valent iron (Fe^0) and phosphorous, to enhance biochar's stability in an aqueous solution [25, 26]. When Fe^0 is attached to the biochar, the material becomes more efficient in removing different organic and inorganic pollutants [26]. Likewise, enriching biochar with other mineral elements can result in improved characteristics. Adding phosphorus into biochar can also enhance the efficiency and effectiveness of biochar due to the addition of a negative charge from the phosphate group [6]. Furthermore, phosphate as an anion

helps to immobilize the heavy metals in an aqueous solution, including Cu^{+2} [27].

This study proposes using orchard waste to synthesize biochar and then modify the synthesized biochar to produce zero-valent iron composited and phosphorus embedded biochar. The adsorption behaviour of the produced adsorbent to scavenge Cu(II) from aqueous media was analysed through pH, kinetics, and equilibrium sorption batch trials. Furthermore, various isotherm and kinetics models were utilized to predict the operating sorption mechanism responsible for removing Cu(II) from aqueous solutions.

2 Materials and Methods

2.1 Adsorbents

2.1.1 Biochar Production

Orchard waste comprising leaves and stems of trees was collected, washed, dried in the air, and cut into pieces. A known amount of prepared feedstock (FS) was placed in a stainless-steel container (7 cm diameter and 22 cm in height), and pyrolysis was completed in an electric muffle furnace. The pyrolysis temperature was maintained at 600 °C for 3 h by keeping the air supply controlled to synthesize biochar. After the accomplishment of the pyrolysis, the biochar sample was allowed to cool in the furnace overnight. The yield of the biochar (BC) after pyrolysis is calculated by using Eq. 1.

$$Yield(\%) = \frac{\text{Weight of biomass} - \text{Weight of biochar}}{\text{Weight of biomass}} * 100$$

(1)

2.1.2 Biochar-Zero-valent Iron Composite Synthesis

The biochar was modified by synthesizing its composites with zero-valent iron by following the procedure reported by Ahmad et al. [6]. The produced BC was washed with deionized (DI) water thrice, ground, and dried at 80 °C in an oven for 24 h. The washed BC was modified with zero-valent iron (Fe^0) particles. Specifically, 50 mL of 1 M $FeSO_4 \cdot 7H_2O$ was mixed in 2.8 g of BC in ethanol/deionized water solution (4:1 v/v ratio). The pH of the suspension was adjusted to 5, stirred for 2 h, and purged under N_2 supply. A 50 mL solution of 2 M $NaBH_4$ was added drop-wise into the suspension under vigorous stirring and N_2 purging. Chitosan was added into the suspension as a binding agent and activated with a 1.2% NaOH solution under stirring. The suspension was left for 12 h, the produced precipitated material (BC/Fe^0) was collected, washed with ethanol, and vacuum dried.

2.1.3 Biochar-Phosphorus Composite Synthesis

Phosphorus (P) composited biochar was fabricated by loading P onto biochar [6]. A solution of 0.001 N phosphorus was mixed with 10 g of BC to acquire P embedded BC. The suspension was stirred until equilibrium at 180 rpm and room temperature (23 ± 2). Subsequently, filtration of the suspension was performed by using Whatman 42 filter paper to separate the BC. The P embedded BC (BC/P) was washed with deionized water to remove surplus P and dried at 65 °C in an oven. The amount of P in the filtrate was analysed through the molybdate-ascorbic acid method using UV/Vis spectrophotometer [CE7400, ©Cecil Instrumentation Services Ltd., Cambridge, UK] [28]. The amount of P adsorbed on the BC is estimated by using Eq. (2).

$$Q_e = \frac{V}{m}(C_o - C_t) \tag{2}$$

where Q_e is the amount of adsorbate, adsorbed (mg g^{-1}), C_o and C_t are the initial and equilibrium adsorbate concentrations (mg L^{-1}), respectively, m is the mass of adsorbent (g), and V is the volume of solution (L).

2.1.4 Commercial Activated Carbon

Peat derived commercially available activated carbon was purchased from Sigma-Aldrich.

2.2 Characterization

The electrical conductivity (EC) and pH of produced adsorbents were analysed in 1:10 (w/v) suspension in deionized water, while the cation exchange capacity (CEC) was determined by NH^{4+}–Na$^+$ method. The total and available contents of P in BC and BC/P were extracted through the digestion, and AB-DTPA method and analysed on UV/Vis spectrophotometer [29, 30]. The different features of the adsorbents, including moisture, ash contents, and volatiles, were determined via ASTM D1762-84 ASTM, 1989), whereas the fixed carbon was estimated through different method. The Fourier transforms infrared spectroscopy (FTIR: Bruker Alpha-Eco ATR-FTIR, Bruker Optics Inc.) was used to analyse the functional groups on the surface, while X-ray diffractometer (XRD: JEOL, JDX 3500) was used to analyse the mineral composition of the adsorbents.

2.3 Cu(II) Adsorption Batch Experiments

2.3.1 Effect of pH and Adsorbent Dose

The pH of the aqueous solution is one of the critical factors affecting removing metals from wastewater. The stock solution of Cu(II) was prepared in DI water, and different concentrations ranging from 50 to 400 mg L^{-1} (50, 100, 200, and 400 mg L^{-1}) of Cu(II) were prepared with initial pH of 4, 7, and 10. About 40 mL of the Cu(II) solution after pH adjustment was taken into polypropylene tubes, and 0.04 g of the adsorbents was suspended into it. Each adsorbent, including blank, was tested in triplicates. The suspension was stirred on a mechanical shaker at 180 rpm under room temperature (23 ± 2 °C) until equilibrium. The solution was separated from the adsorbents by filtering through Whatman 42 filter paper. The amount of Cu(II) remaining in the filtrate was analysed through the atomic absorption spectrophotometer (novAA® 400 P, Analytik Jena, Germany). The amount of Cu(II) adsorbed onto the adsorbent under each pH condition is estimated by using Eq. (2). The initial pH 4 was observed as optimum for Cu(II) onto the tested adsorbents.

For the dose optimization, a solution having 400 mg L^{-1} of Cu(II) with an initial pH of 4 was selected. 40 mL from this solution was taken into a polypropylene tube, and an adsorbent dose of 0.1–1 g L^{-1} was suspended. Each adsorbent, including blank, was tested in triplicates. The suspension was shaken at 180 rpm under room temperature (23 ± 2 °C) until equilibrium, and the concentration of Cu(II) in the filtrates was measured after filtering through Whatman 42 filter paper.

2.3.2 Kinetics Batch Adsorption

Cu(II) solution of 400 mg L^{-1} concentration with an initial pH of 4 was taken into a polypropylene tube, and 0.04 g of the adsorbent was suspended into it. The suspension was shaken at 180 rpm under room temperature (23 ± 2 °C). Each adsorbent along with blank was drawn from the shaker in triplicates after every 15 min interval. The kinetics batch test was performed for different time intervals ranging from 0 to 120 min. The solutions were separated by filtering through Whatman 42 filter paper from the adsorbents, and the concentration of Cu(II) in the filtrates was measured. The amount of Cu(II) adsorbed onto the adsorbents is calculated using Eq. (2).

2.3.3 Isotherm Batch Adsorption

Various solutions with initial Cu(II) concentrations of 10, 50, 100, 200, and 400 mg L^{-1} and pH of 4 were repapered in deionized water. 0.04 g of each adsorbent, along with blank, was suspended into 40 mL of each of the solutions in a polypropylene tube. Each adsorbent and blank were repeated thrice. The suspensions were shaken at 180 rpm under room temperature (23 ± 2 °C) for 120 min. The adsorbents were separated from the solutions, and the concentration of Cu(II) in the solution was analysed. The adsorbed amount of Cu(II) is found by using Eq. (2).

2.4 Quality Control

All the Cu(II) solutions were prepared in DI water using $CuSO_4 \cdot 5H_2O$ (99.5%) purchased from DaeJung Chemicals, Korea. All treatments were replicated thrice for the accuracy of results. The filtrates were filtered again using 0.45 μm nylon syringe filters and before running on atomic absorption spectrophotometer. The Cu(II) standards were run onto the atomic absorption spectrophotometer as unknown samples, and the acquired recovery was 94–106%.

3 Results and Discussion

3.1 Characterization and Proximate Analysis

The properties of the synthesized adsorbents (chemical and proximate) are shown in Table 1. The yield of the produced biochar was 39.51%. The FS showed the highest volatiles contents (66.22%), while minimum volatiles (10.95%) were observed in BC due to the feedstock's thermal treatment. The volatiles increased to 14.51% and 21.12% in BC/P and BC/Fe^0, respectively, due to BC's modification. The highest fixed carbon contents were exhibited by BC (53.42%) and BC/P (52.06%) due to the feedstock's carbonization as a result of the thermal process. The lowest fixed carbon (16.05%) and highest ash contents (59.85%) of the BC/Fe^0 were due to Fe contents in the materials, which remained integrated and confounded with ash contents. The pyrolysis process resulted in a 4 unit increment in pH of BC due to alkaline functional groups' condensation and removal of acid functional groups [31]. However, the pH increases in BC/Fe^0 and BC/P was only 2 and 3 unit, respectively, which could be due to washing out of alkaline functional groups during the biochar modification process.

The reduction in cation exchange capacity (CEC) from 73.51 cmol kg^{-1} in FS to 42.25 cmol kg^{-1} in BC could be due to the removal of surface functional groups and enhanced aromaticity as a result of thermalization [32]. Further decrease in CEC (28.96 cmol kg^{-1}) in BC/P could be due to adsorption of P onto the exchange cites, whereas increment in the CEC (65.88 cmol kg^{-1}) of BC/ Fe^0 could be due to the presence of nano-sized Fe^0 particles. Biochar having higher CEC has shown high adsorption capacities [33, 34].

The XRD patterns of the orchard waste feedstock, pristine, and modified biochar are presented in Fig. 1. A peak with higher intensity at 21.3° in FS depicted the occurrence of cellulose in biomass. However, this peak disappeared with pyrolysis in BC, BC/Fe^0, and BC/P, due to degradation of cellulosic materials in biomass. A peak appearing at 20.9° in BC/P was designated to brushite ($CaHPO_4 \cdot 2H_2O$), which could have formed after the interaction of P with Ca in

Table 1 The analyses (proximate and chemical) of orchard waste feedstock (FS), its derived biochar (BC), phosphorus embedded BC (BC/P), zero-valent iron composited BC (BC/Fe^0) and activated carbon (AC)

| Materials | Proximate analyses | | | | | Chemical analyses | | | | |
	Yield (%)	Moisture (%)	Volatiles (%)	Fixed carbon (%)	Ash (%)	pH	Electrical conductivity (dS m^{-1})	Cation exchangeable capacity (cmol kg^{-1})	Total P (mg kg^{-1})	Available P (mg kg^{-1})
FS	–	3.92 ± 0.51	66.22 ± 3.21	18.47 ± 2.32	11.39 ± 2.11	5.02 ± 0.82	11.51 ± 0.98	73.51 ± 3.21	998.36 ± 32.18	59.74 ± 3.54
BC	39.51 ± 3.11	2.11 ± 0.12	10.95 ± 2.23	53.42 ± 5.13	33.52 ± 2.13	9.91 ± 0.98	5.35 ± 0.23	42.25 ± 3.25	1032.66 ± 53.58	63.84 ± 5.65
BC/Fe^0	–	2.98 ± 0.21	21.12 ± 2.15	16.05 ± 1.65	59.85 ± 5.30	7.03 ± 0.52	3.11 ± 0.35	65.88 ± 5.32	–	–
BC/P	–	0.85 ± 0.11	14.51 ± 1.23	52.06 ± 5.27	32.58 ± 2.10	7.82 ± 0.25	1.22 ± 0.27	28.96 ± 3.128	3856.41 ± 45.54	2787.83 ± 27.33
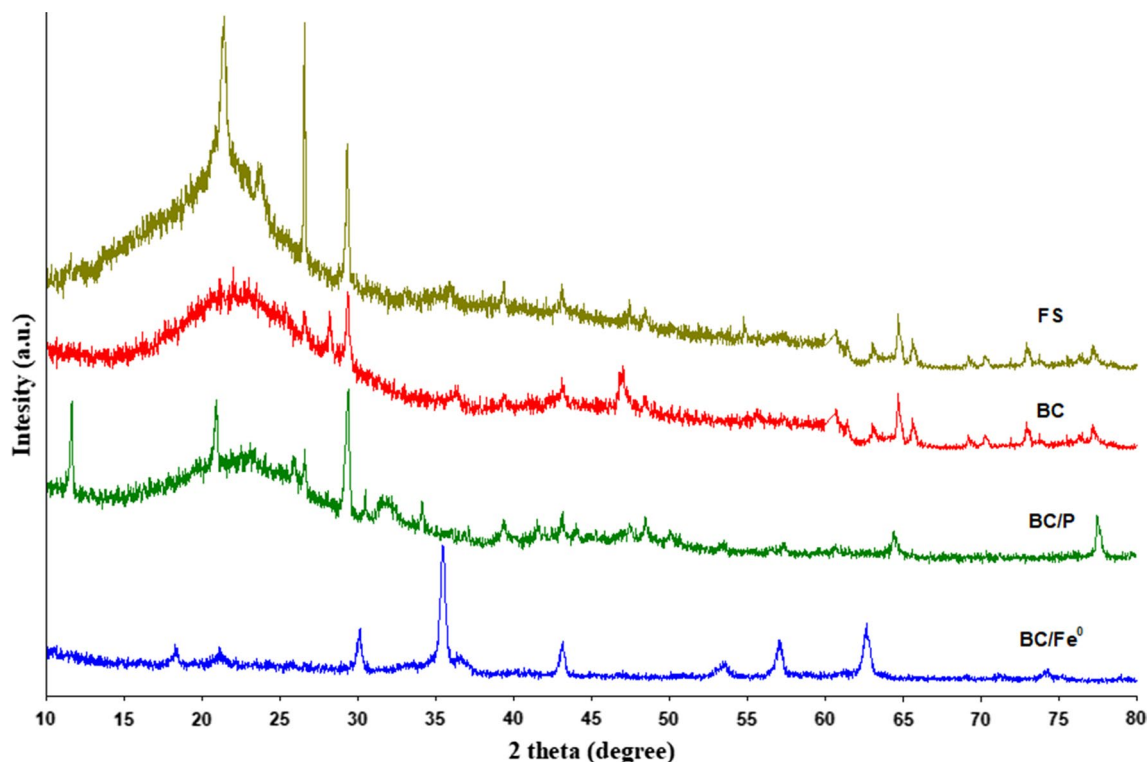
Fig. 1 X-ray diffraction (XRD) analyses patterns of orchard waste feedstock (FS), its derived biochar (BC), phosphorus embedded BC (BC/P), and zero-valent iron composited BC (BC/Fe^0)

biochar matrix [35]. The P loadings on the surface of the biochar can be evidenced by the occurrence of $CaHPO_4 \cdot 2H_2O$ at 11.6° and a peak of hydroxyapatite at 30.5° in BC/P [36]. Likewise, the successful composite formation in BC/Fe^0 can be confirmed by peaks at 43° and 63° ascribing as zerovalent iron particles [31, 37–39].

The obtained FTIR spectra of the tested materials are shown in Fig. 2. A band around 3300 cm^{-1} in FS was due to the O–H stretching of H-bonding due to free moisture contents, which was lost upon thermal treatment in the rest of the materials [31]. Similarly, the O–H and aliphatic C–H stretch bands at 2810 and 2890 cm^{-1} in FS were absent in other materials.

Broadband with lower transmittance at 1618 cm^{-1} was due to the presence of –COOH groups such as esters, ketones, and carboxyl in FS, while a band at 1095 cm^{-1} in all the materials was owing to C–O–C stretches. The existence of Fe^0 particles can be evidenced by the presence of a band at 3421 cm^{-1} which was ascribed as –OH stretching vibration resulted from the generation of FeOOH layer on iron particles [40].

### 3.2 Effect of pH on Cu(II) Removal

The effects of initial solution pH of 4, 7, and 10 on Cu(II) removal by the tested adsorbents were studied with initial Cu(II) concentrations of 50, 100, 200, 400 mg L^{-1}, and the obtained results are presented in Fig. 3. Although the initial concentration of Cu(II) is different in each graph, its adsorption trend is similar. The per cent removal was less at pH 4, which increased with increase in pH 8. With further increase in pH beyond 8, the Cu(II) removal was decreased significantly. Therefore, results revealed that pH 7–8 was optimum for higher Cu(II) removal by the studied adsorbents. Considering the initial Cu(II) concentration, the higher per cent removal was observed with 50 mg L^{-1}, which reduced subsequently with rising in initial Cu(II) concentration in the solution.

The lower adsorption of Cu(II) onto the adsorbents at lower solution pH could be due to the electrostatic repulsion between the H$^+$ groups present on the material surface and the positively charged Cu(II) ion [41]. The increase in solution pH towards neutral has resulted in the hydrolysis of Cu(II) to form Cu(OH)$^+$, subsequently adsorbing more Cu(II) ions onto the synthesized material [3]. However, a further rise in solution pH above neutral caused the formation of Cu(OH)$_2$ precipitates and therefore resulting in lower Cu(II) adsorption [3]. Thus, the results revealed that a neutral pH was optimum for the highest Cu(II) onto the tested adsorbents.
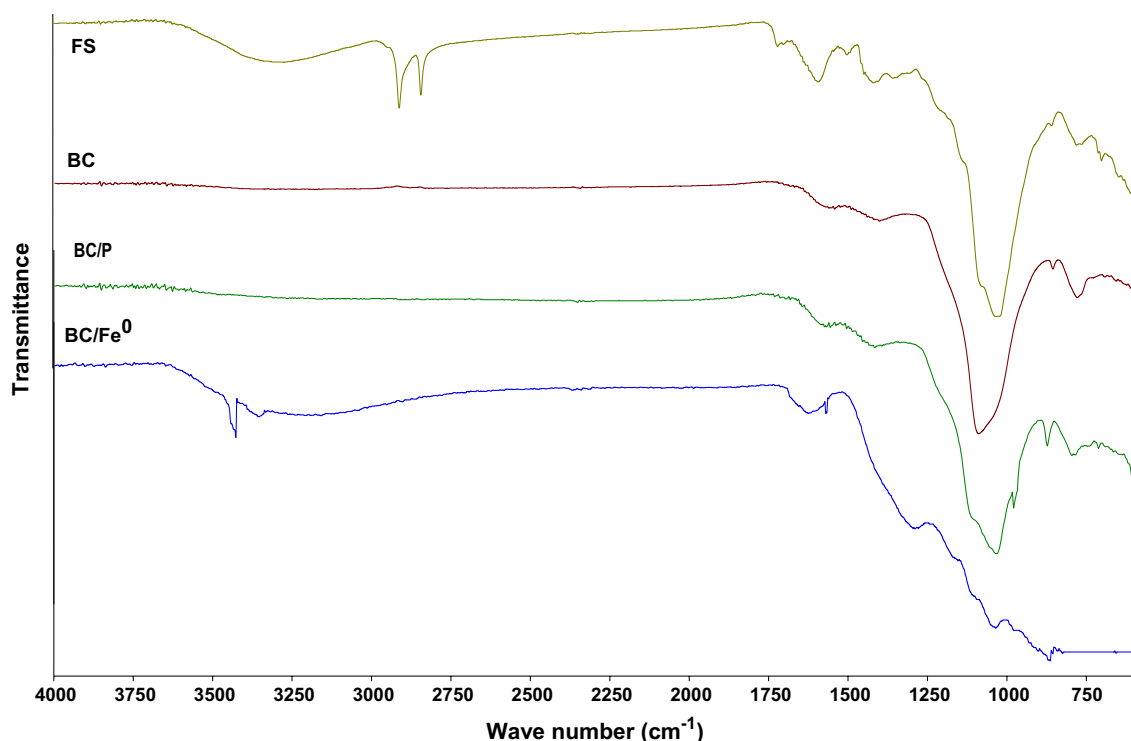
Fig. 2 Fourier transform infrared spectroscopy (FTIR) spectra of orchard waste feedstock (FS), its derived biochar (BC), phosphorus embedded BC (BC/P), and zero-valent iron composited BC (BC/Fe^0)

3.3 Kinetics of Cu(II) Sorption

Kinetics sorption batch trials were conducted at a constant temperature, pH, and initial Cu(II) concentrations to investigate the tested adsorbents' sorption dynamics towards Cu(II). Different kinetics models including first-order, second-order, pseudo-first-order, pseudo-second-order, Elovich, intraparticle diffusion, and power function (Eqs. 3–9, respectively) were applied to the sorption data to understand the dynamics of Cu(II) adsorption onto the tested adsorbents. The standard error of estimate (SEE) is calculated by using Eq. 10.

$$\ln q_t = \ln q_o - k_1 t \tag{3}$$

$$\frac{1}{q_t} = \frac{1}{q_o} - k_2 t \tag{4}$$

$$\ln\left(q_e - q_t\right) = \ln q_e - k_1' t \tag{5}$$

$$\frac{t}{q_t} = \frac{1}{k_2' q_e^2} + \frac{1}{q_e} t \tag{6}$$

$$q_t = \frac{1}{\beta} \ln\left(\alpha\beta\right) + \frac{1}{\beta} \ln t \tag{7}$$

$$\ln q_t = \ln b + k_f(\ln t) \tag{8}$$

$$q_t = c + k_{id} t^{0.5} \tag{9}$$

$$\text{SEE} = \sum_{i=1}^{n} \left(q_{em} - q_{ec}\right)^2 \tag{10}$$

where q_o and q_t are the amounts of Cu(II) sorbed (mg g^{-1}) at time 0 (min) and time t, respectively. q_e is the sorption capacity at equilibrium (mg g^{-1}). k_1 and k_1' are the first- and pseudo-first-order rate constants. k_2 and k_2' are the second- and pseudo-second-order rate constants, respectively. α and β are sorption rates (mg g^{-1} min^{-1}). k_{id} is the apparent diffusion rate constant (in [mg g^{-1}]$^{-0.5}$), and c is the diffusion constant. q_{em} and q_{ec} are measured and calculated Cu(II) sorption capacities (mg g^{-1}) of the adsorbents, and n is the number of measurements.

The sorption dynamics of the kinetics, as presented in Fig. 4, shows three distinct sorption stages, i.e. initial rapid sorption stage, relatively slower sorption stage, and equilibrium stage. It is evident from Fig. 4 that BC/Fe^0 was the quicker one to acquire an equilibrium stage, followed by BC, AC, and BC/P. Based on the R^2 and SEE values calculated from kinetics models, the suitability of the models was in the order of Elovich > pseudo-second-order > intraparticle
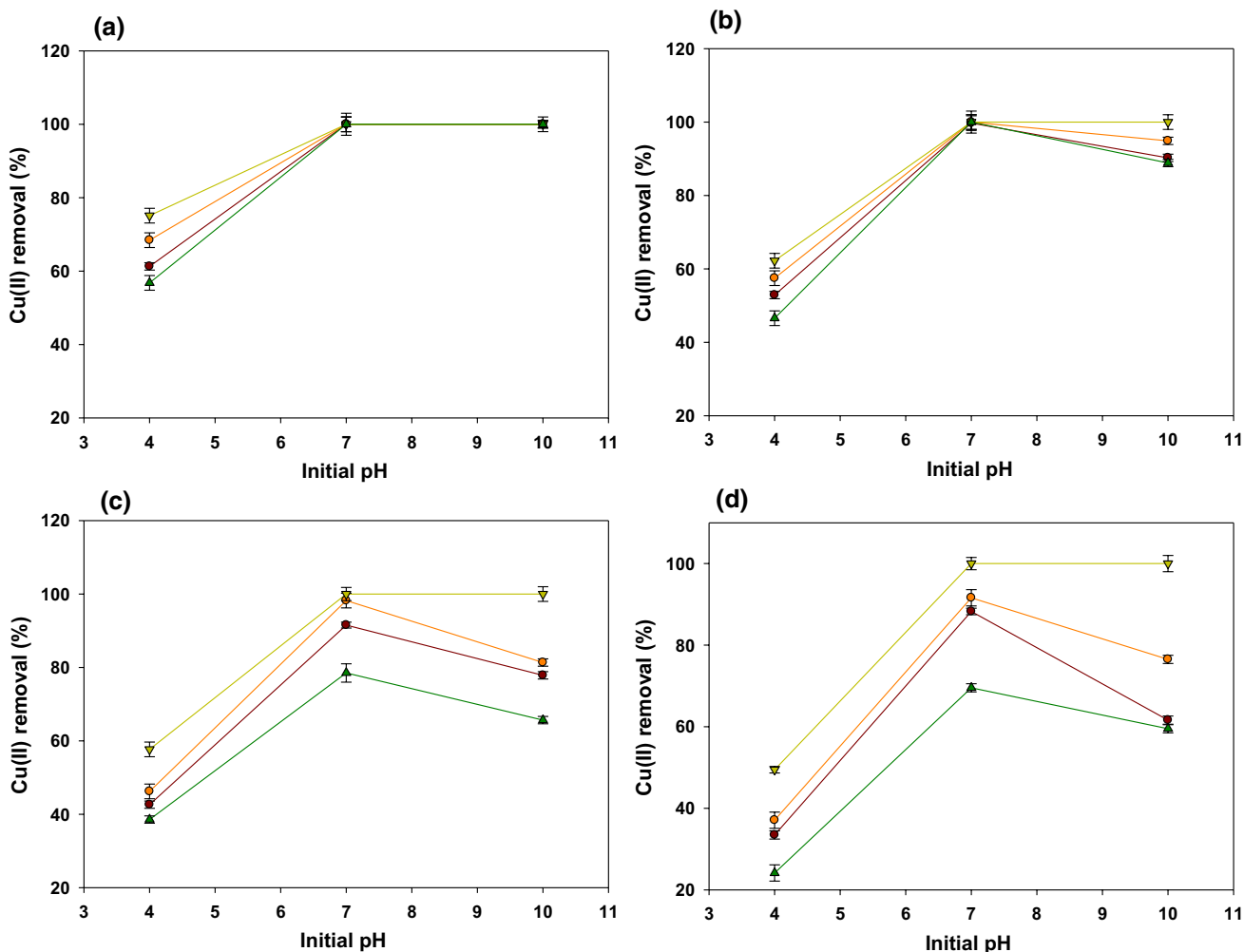
Fig. 3 Effect of pH on the adsorption Cu(II) onto orchard waste-derived biochar (BC), phosphorus embedded BC (BC/P), zero-valent iron composited BC (BC/Fe^0), and activated carbon (AC). The initial Cu(II) concentrations in the aqueous solutions were **a** 50 mg L^{-1}, **b** 100 mg L^{-1}, **c** 200 mg L^{-1}, and **d** 400 mg L^{-1}
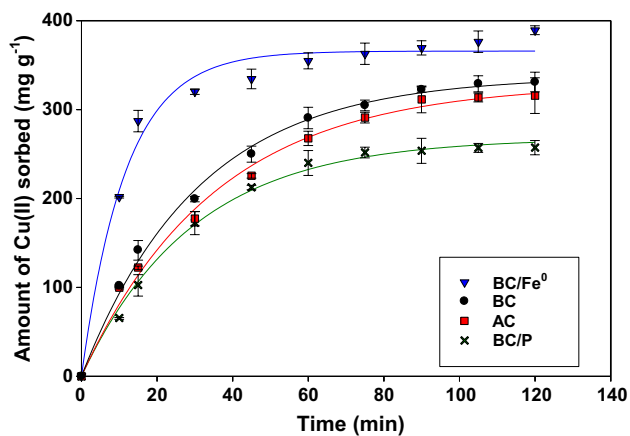
Fig. 4 Copper [Cu(II)] sorption kinetics onto orchard waste biochar (BC), phosphorus embedded BC (BC/P), zero-valent iron composited BC (BC/Fe^0), and activated carbon (AC)

diffusion > power function > pseudo-first-order > first-order second-order (Table 2). Second-order, first-order, and pseudo-first-order were inappropriate to ascribe the Cu(II) sorption onto the synthesized material. Overall, the highest value of R^2 of BC/Fe^0 (0.976), BC (0.966), AC (0.950), and BC/P (0.945) suggested that the Elovich model was best fitted for the Cu(II) sorption onto the synthesized material. Moreover, intraparticle diffusion, power function, and pseudo-second-order kinetics models were also fitted for Cu(II) ions sorption. The best fitness of the Elovich and pseudo-second-order kinetics models suggested chemisorption, while the fitness of intraparticle diffusion further depicted the involvement of diffusion process in the adsorption of Cu(II) onto synthesized adsorbents.

The kinetic parameters obtained from Cu(II) sorption dynamics are shown in Table 3. The initial sorption rate of Elovich model (α) was 79.44, 75.71, 72.28,

Table 2 Coefficient of determination (R^2) and standard errors of estimate (SEE) of kinetic models for copper (Cu(II)) adsorption onto orchard waste-derived biochar (BC), phosphorus embedded BC (BC/P), zero-valent iron composited BC (BC/Fe^0), and activated carbon (AC)

Sorbent	First-order		Second-order		Pseudo-first-order		Pseudo-second-order		Elovich		Intraparticle diffusion		Power function	
	R^2	SEE	R^2	SEE	R^2	SEE	R^2	SEE	R^2	SEE	R^2	SEE	R^2	SEE
BC/Fe^0	0.584	0.0185	0.002	0.6367	0.583	0.1370	0.923	0.0014	0.976	0.0040	0.823	0.0011	0.771	0.0001
BC	0.833	0.0097	0.122	0.0004	0.834	0.0097	0.965	0.0014	0.966	0.0028	0.972	6.4×10^{-5}	0.872	0.0007
AC	0.863	0.0035	0.139	0.0008	0.862	0.0035	0.950	0.0026	0.950	0.0009	0.980	0.0100	0.873	0.0003
BC/P	0.785	0.0080	0.138	0.0008	0.785	0.0800	0.952	0.0673	0.945	0.0048	0.940	0.0086	0.892	0.0004

61.60 mg g^{-1} min^{-1} in comparison with the pseudo-second-order (h) which provided 53.61, 19.45, 16.57, 14.85 mg g^{-1} min^{-1} for BC/Fe^0, BC, AC, and BC/P, respectively.

Furthermore, a greater Cu (II) sorption rate has been observed onto BC/Fe^0 composite than the other synthesized material. Similarly, the Elovich model predicted β was highest in BC/Fe^0 (24.82), whereas all other adsorbents generated negative β values. Likewise, the higher rate constants in case of power function ($b = 1.4088$) and intraparticle diffusion ($k_{id} = 30.77$ [mg g^{-1}] $- 0.5$) for BC/Fe^0 composite suggested that it needed a short time to sorb Cu(II) ions as compared to other materials. Interestingly, pseudo-second-order predicted maximum Cu(II) adsorption capacity of BC/Fe^0, which was 4.1 [36], 4.2, and 5 times higher as compared to BC, AC, and BC/P, respectively. Based on the sorption dynamics, it was shown that Elovich, intraparticle diffusion models, and pseudo-second-order well described the sorption of Cu(II) onto the tested adsorbents in order of BC/Fe^0 > BC > AC > BC/P [36].

3.4 Equilibrium Cu(II) Sorption

Equilibrium batch experiments were carried out to find the synthesized materials' sorption efficiencies for Cu(II) ions. Langmuir, Freundlich, Redlich–Peterson, Temkin, and Dubinin–Radushkevich models were applied to investigate the sorption pattern of Cu(II) ions adsorbed on the synthesized material. The nonlinear forms of the models were applied to avoid the error variance. The adsorption data analysed by various isotherm models are as follows [40, 42]:

$$q_e = K_F C_e^{1/n} \tag{11}$$

$$q_e = \frac{Q_L C_e K_L}{1 + K_L C_e} \tag{12}$$

$$q_e = \frac{AC_e}{1 + BC_e^g} \tag{13}$$

$$q_e = \frac{RT}{b} \ln (AC_e) \tag{14}$$

$$q_e = q_D \exp \left(-B_D \left[RT \ln \left(1 + \frac{1}{C_e} \right) \right]^2 \right) \tag{15}$$

where K_F (L g^{-1}) is the sorptive affinity parameter, and $1/n$ is the component related to linearity in Freundlich isotherm. Q_L (mg g^{-1}) and K_L (L mg^{-1}) are Langmuir maximum adsorption capacity and sorption equilibrium constant, respectively. A (L g^{-1}) and B (L mg^{-1}) are the constants in Redlich–Peterson equation, and exponent g has the value between 0 and 1. In Temkin isotherm equation, b is a heat of adsorption and A is binding constant (L mg^{-1}) q_D is the maximum adsorption capacity of the adsorbent (mg g^{-1}) in Dubinin–Radushkevich model.

Table 3 Parameters obtained from kinetic models for copper Cu(II) adsorption onto orchard waste-derived biochar (BC), phosphorus embedded BC (BC/P), zero-valent iron composited BC (BC/Fe^0) and activated carbon (AC)

Sorbent	First-order	Second-order	Pseudo-first-order		Pseudo-second-order			Elovich		Intraparticle diffusion		Power function	
	k_1	k_2	k_1'	q_e	k_2'	q_e	h	A	β	k_{id}	c	k_f	b
BC/Fe^0	0.0235	-4.1×10^{-7}	-0.0443	5.660	2.3×10^{-7}	1538.2	53.61	79.44	24.82	30.77	95.43	1.0999	1.4088
BC	0.0265	-2.2×10^{-5}	-0.0507	6.188	1.3×10^{-4}	383.57	19.45	75.71	-34.68	31.98	14.97	1.1230	1.0339
AC	0.0267	-2.5×10^{-5}	-0.0525	6.125	1.1×10^{-4}	373.15	16.57	72.28	-37.47	30.89	7.581	1.1157	0.9941
BC/P	0.0263	-3.7×10^{-5}	-0.0537	5.755	1.6×10^{-4}	307.50	14.85	61.60	-31.68	25.85	9.873	1.0990	0.8972

The bonding energy (E) for the ion-exchange mechanism can be calculated based on the mean free energy of sorption (B_D) by using Eq. 16.

$$E = \frac{1}{\sqrt{2B_D}} \tag{16}$$

The adsorption isotherm of the employed models (Fig. 5) showed that the sorption of Cu(II) on the adsorbent materials was increased by increasing the initial Cu(II) concentration [31]. It has previously been reported that the pollutant's initial concentration decided the type of equilibrium isotherms [43, 44]. The adsorption of Cu(II) was very high at initial low concentration (up to 50 mg L^{-1}). The strong adsorbate–adsorptive interactions helped to develop an H-type isotherm showing the presence of more active sites. Above 50 mg L^{-1}, adsorption was less due to less active site forming an L-shaped isotherm [36]. All the isotherm models exhibited a similar trend with higher adsorption capacity of BC/Fe^0, followed by BC, AC, and BC/P. Nonlinear parameters obtained from the applied isotherm models are shown in Table 4. The Langmuir, Freundlich, and Redlich–Peterson models were fitted well to the Cu(II) adsorption data by showing high R^2 values (0.999–0.968), while Temkin and Dubinin–Redushkecih models were not fitted well as R^2 values were in the range of 0.915–0.832 and 0.904–0.857, respectively.

The Langmuir isotherm describes monolayer adsorption, Freundlich isotherm describes multilayer chemical adsorption of adsorbate onto the adsorbent, and the Redlich–Peterson model combines the features of both Langmuir and Freundlich isotherm models [45]. The best fitness of Langmuir, Freundlich, and Redlich–Peterson models to the Cu(II) adsorption data suggested both mono- and multilayer adsorption of Cu(II) onto the tested adsorbents. The Cu(II) ions are adsorbed chemically either by making electron sharing, covalent bond, or adsorption in the adsorbate's pores [42, 46, 47]

The Langmuir model's suitability is well described for the structurally homogeneous adsorbent where all the available sites are alike and have equal energy. The Langmuir model projected maximum adsorption capacity (Q_L) in the order BC/Fe^0 (427.11 mg g^{-1}) > BC (204.72 mg g^{-1}) > AC (198.64 mg g^{-1}) > BC/P (121.56 mg g^{-1}). Likewise, the Freundlich isotherm generated K_F followed a similar trend by yielding the highest value for BC/Fe^0 (6.2252 L g^{-1}), followed by BC (5.4242 L g^{-1}), AC (4.3101 L g^{-1}), and BC/P (3.0308 L g^{-1}). The highest value of K_F for BC/Fe^0 suggested the highest Cu(II) adsorption onto this adsorbent due to the excess of active sites [31]. The g value obtained from Redlich–Peterson isotherm was in a range of 0.4826–0.5968 for all the adsorbents, suggesting that the limitation of Freundlich isotherm was less than that of Langmuir.

Furthermore, the lowest g value (0.3703) was obtained for BC/Fe^0, suggesting the highest Cu(II) adsorption onto the said adsorbent due to strong attraction of BC/Fe^0 ions converting it into inorganic oxides after interacting with oxygen-containing functional groups in the organic backbone. Moreover, the enhanced surface coverage of biochar with Fe^0/Fe$_3$O$_4$ crystals, providing more adsorption sites, could increase the adsorption of Cu(II) by transferring into H–Fe–O–M^{n+} species in an aqueous solution [47]. In contrast, the conditions became unfavourable at high initial concentrations due to surface loading and saturation of pore space [18]. The highest Cu(II) adsorption capacity of BC/Fe^0 could be due to synergy of nano-sized iron particles and biochar, surface complexes with available –OH/–COOH functional groups, and/or delocalized π electrons into the biochar matrix [47].

The suitability of the Cu(II) adsorption onto the tested adsorbents was further assessed using the Freundlich model predicted 1/n. The predicted 1/n values in Freundlich isotherm were in the range of 0.4250–0.6750 (< 1), indicating the appropriate Cu(II) adsorption in case of all the adsorbents. Furthermore, the lowest 1/n values for BC/Fe^0 indicated the highest Cu(II) adsorption onto this material. Additionally, the Langmuir model derived separation factor (R_L) may be used to determine the affinity between adsorbate and adsorbent by using Eq. 17 [48]

$$R_L = \frac{1}{1 + K_L C_o} \tag{17}$$

Figure 6 represents that the values for all the tested adsorbents were less than unity, suggesting the appropriateness of Cu(II) adsorption. Thus, the isotherm data results indicated that the synthesized materials were suitable for the removal of Cu(II) from aqueous waste media.

3.5 Proposed Mechanism

pH, kinetics, and isotherm batch sorption experiments were conducted to investigate the synthesized adsorbents' sorption efficiency against Cu(II). The best fitness of Elovich and pseudo-second-order kinetic models suggested that chemisorption was the dominant sorption mechanism for Cu(II) adsorption onto the tested adsorbents. It could be due to positively charged Cu(II) ions with the surface functional groups present on the adsorbents' surface, which might have involved the electron exchange between adsorbent and adsorbate [40, 47]. Additionally, intraparticle diffusion's best fitness suggested that Cu(II) ions were also diffused into the porous structure of the adsorbents. These results are also in agreement with the best fitness of Freundlich, Langmuir, and Redlich–Peterson isotherm, suggesting that the adsorption of Cu(II) onto the tested adsorbents were being
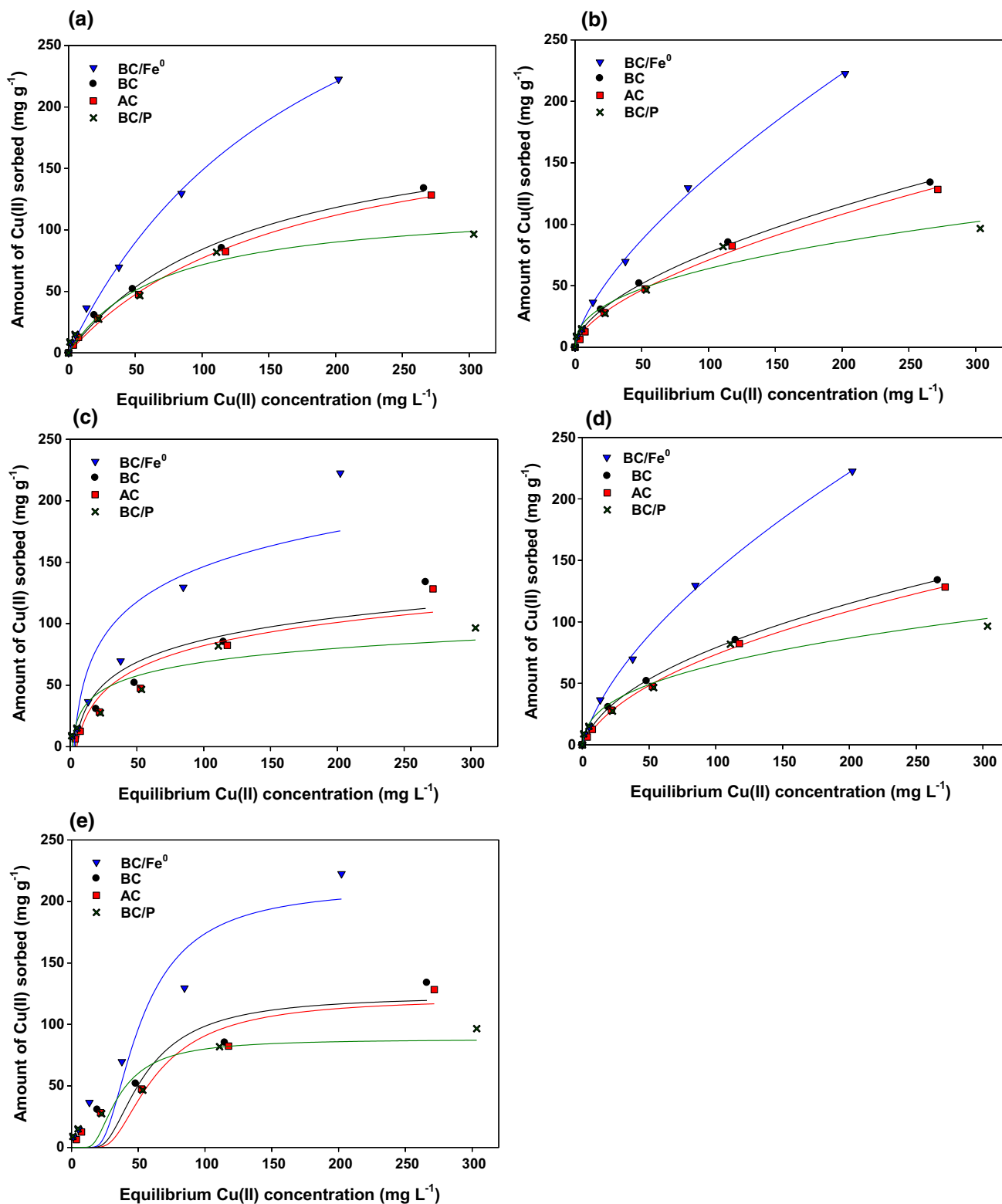
Fig. 5 Copper [Cu(II)] sorption isotherms fittings on **a** Langmuir, **b** Freundlich, **c** Temkin, **d** Redlich–Peterson, and **e** Dubinin–Radushkevich models by orchard waste feedstock (FS), its derived biochar (BC), phosphorus embedded BC (BC/P), zero-valent iron composited BC (BC/Fe^0), and activated carbon (AC)

Table 4 Nonlinear parameters of Langmuir, Freundlich, Temkin, Dubinin–Radushkevich, and Redlich–Peterson isotherms are indicating copper [Cu(II)] adsorption onto orchard waste-derived biochar (BC), phosphorus embedded BC (BC/P), zero-valent iron composited BC (BC/Fe^0), and activated carbon (AC)

Isotherms	Parameters	BC	AC	BC/Fe^0	BC/P
Langmuir	Q_L (mg g^{-1})	204.72	198.64	427.11	121.56
	K_L (L g^{-1})	0.0060	0.0073	0.0053	0.0143
	R^2	0.998	0.998	0.999	0.989
Freundlich	K_F (L g^{-1})	5.4242	4.3101	6.2252	3.0308
	$1/n$	0.5759	0.6081	0.3750	0.7250
	R^2	0.995	0.993	0.991	0.968
Redlich–Peterson	A (L g^{-1})	2.7327	3.7655	1.9134	8.6909
	B (L mg^{-1})^g	0.1185	0.0627	0.1310	0.7538
	G	0.4859	0.4826	0.3703	0.5968
	R^2	0.992	0.994	0.995	0.969
Temkin	b (J mol^{-1})	27.235	26.182	41.353	16.170
	A (L g^{-1})	0.2757	0.2043	0.3451	0.7043
	R^2	0.894	0.915	0.832	0.864
Dubinin–Radushkevich	Q_D (mg g^{-1})	123.39	121.52	212.13	88.048
	E (kJ g^{-1})	0.9168	1.190	0.8124	0.3911
	R^2	0.857	0.875	0.904	0.872
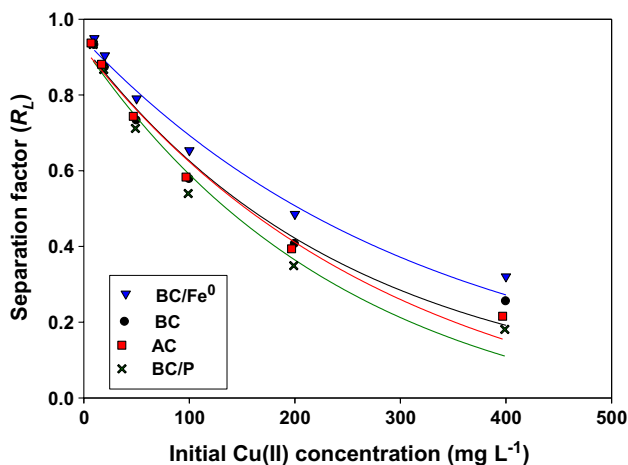
Fig. 6 Separation factor (RL) obtained from Langmuir isotherms versus initial Cu(II) (copper) concentration for derived biochar (BC), phosphorus embedded BC (BC/P), zero-valent iron composited BC (BC/Fe^0), and activated carbon (AC)

controlled with multiple mechanisms. The mono- and multi-layer chemical adsorption of Cu(II) onto the adsorbents can be explained by the best fitness of Langmuir and Freundlich isotherms, respectively. Moreover, the electrostatic interactions between cationic Cu(II) ions and negatively charged surface functional groups also played a role in Cu(II) adsorption near neutral pH. In contrast, the precipitation of Cu(II) can occur in pH above 7 [49]. The precipitation is an essential mechanism for heavy metal removal from aqueous media; however, to remove precipitated salts at lower concentration might be challenging [50]. The higher Cu(II) adsorption onto BC/Fe^0 could be due to the higher surface area and larger pore size of the said adsorbent due to nano-sized iron particles, which provided more active adsorption sites. Therefore, it can be concluded that the adsorption of Cu(II) onto the synthesized adsorbents was mainly being controlled by chemisorption (Cu(II) adsorption O-containing functional groups of hydrophilic sites), physisorption (diffusion into the pore), electrostatic interactions, and precipitation (above pH 7).

4 Conclusions

The ecofriendly and renewable orchard waste biochar (BC) in pristine form and modified with zero-valent iron (BC/Fe^0) and phosphorus (BC/P) was used to check the selectivity and removal of Cu from the aqueous solution. A comprehensive and systematic mechanism was deliberated for Cu removal in aqueous solution at different pH levels. The oxidation-resistant BC/Fe^0 biochar proved to be highly efficient due to its mono- and multilayer sorption capability for Cu(II) removal. The existence of additional functional groups on the BC/Fe^0 helped increase biochar's adsorption capacity on acidic and neutral pH. The results were best fitted in the Elovich model and Langmuir isotherm. BC/Fe^0 also found the highest adsorption capacity (427.11 mg g^{-1}) among other adsorbents. The higher Cu(II) adsorption using BC/Fe^0 was due to the large surface area as the presence of nano-sized iron particles provided more active adsorption sites. Overall, the Fe^0 composited orchard waste-derived biochar opened an avenue for multi-metal removal in addition to the Cu(II) from the aqueous solution.

References

1. Nriagu, J.O.: A history of global metal pollution. Science **272**, 223–223 (1996). https://doi.org/10.1126/science.272.5259.223
2. Mushtaq, M.; Bhatti, H.N.; Iqbal, M.; Noreen, S.: Eriobotrya japonica seed biocomposite efficiency for copper adsorption: isotherms, kinetics, thermodynamic and desorption studies. J. Environ. Manag. **176**, 21–33 (2016). https://doi.org/10.1016/j.jenvman.2016.03.013
3. Demiral, H.; Güngör, C.: Adsorption of copper(II) from aqueous solutions on activated carbon prepared from grape bagasse. J. Clean. Prod. **124**, 103–113 (2016). https://doi.org/10.1016/j.jclepro.2016.02.084
4. Zhiani, R.; Saadati, S.M.; Zahedifar, M.; Sadeghzadeh, S.M.: Synthesis of new class of copper(II) complex-based FeNi$_3$/KCC-1 for the N-formylation of amines using dihydrogen and

carbon dioxide. Catal. Lett. **148**, 2487–2500 (2018). https://doi.org/10.1007/s10562-018-2475-4

5. Amin, M.T.; Alazba, A.A.; Shafiq, M.: Removal of copper and lead using banana biochar in batch adsorption systems: isotherms and kinetic studies. Arab. J. Sci. Eng. **43**, 5711–5722 (2018). https://doi.org/10.1007/s13369-017-2934-z

6. Ahmad, M.; Usman, A.R.A.; Al-Faraj, A.S.; Ahmad, M.; Sallam, A.; Al-Wabel, M.I.: Phosphorus-loaded biochar changes soil heavy metals availability and uptake potential of maize (*Zea mays* L.) plants. Chemosphere **194**, 327–339 (2018). https://doi.org/10.1016/j.chemosphere.2017.11.156

7. Rahman, M.S.; Islam, M.R.: Effects of pH on isotherms modeling for Cu(II) ions adsorption using maple wood sawdust. Chem. Eng. J. **149**, 273–280 (2009). https://doi.org/10.1016/j.cej.2008.11.029

8. Demirkiran, N.: Copper adsorption by natural manganese dioxide. Trans. Nonferr. Met. Soc. China **25**, 647–653 (2015). https://doi.org/10.1016/S1003-6326(15)63648-2

9. Mohammed, A.A.; Samaka, I.S.: Bentonite coated with magnetite Fe_3O_4 nanoparticles as a novel adsorbent for copper (II) ions removal from water/wastewater. Environ. Technol. Innov. **10**, 162–174 (2018). https://doi.org/10.1016/j.eti.2018.02.005

10. Donoso, A.; Cruces, P.; Camacho, J.; Ríos, J.C.; Paris, E.; Mieres, J.J.: Acute respiratory distress syndrome resulting from inhalation of powdered copper. Clin. Toxicol. **45**, 714–716 (2007). https://doi.org/10.1080/15563650701438912

11. Lee, J.-S.; Chon, H.-T.; Kim, K.-W.: Human risk assessment of As, Cd, Cu and Zn in the abandoned metal mine site. Environ. Geochem. Health **27**, 185–191 (2005). https://doi.org/10.1007/s10653-005-0131-6

12. Egorova, K.S.; Ananikov, V.P.: Which metals are green for catalysis? Comparison of the toxicities of Ni, Cu, Fe, Pd, Pt, Rh, and Au salts. Angew. Chem. Int. Ed. **55**, 12150–12162 (2016). https://doi.org/10.1002/anie.201603777

13. Shahzad, A.; Rasool, K.; Miran, W.; Nawaz, M.; Jang, J.; Mahmoud, K.A.; Lee, D.S.: Two-dimensional $Ti_3C_2T_x$ MXene nanosheets for efficient copper removal from water. ACS Sustain. Chem. Eng. **5**, 11481–11488 (2017). https://doi.org/10.1021/acssuschemeng.7b02695

14. Hassaan, M.A.; Nemr, A.E.; Madkour, F.F.: Environmental assessment of heavy metal pollution and human health risk. Presented at the (2016)

15. Ahluwalia, S.S.; Goyal, D.: Microbial and plant derived biomass for removal of heavy metals from wastewater. Bioresour. Technol. **98**, 2243–2257 (2007). https://doi.org/10.1016/j.biortech.2005.12.006

16. Wan, M.-W.; Kan, C.-C.; Rogel, B.D.; Dalida, M.L.P.: Adsorption of copper (II) and lead (II) ions from aqueous solution on chitosan-coated sand. Carbohydr. Polym. **80**, 891–899 (2010). https://doi.org/10.1016/j.carbpol.2009.12.048

17. Wah Chu, K.; Chow, K.L.: Synergistic toxicity of multiple heavy metals is revealed by a biological assay using a nematode and its transgenic derivative. Aquat. Toxicol. **61**, 53–64 (2002). https://doi.org/10.1016/S0166-445X(02)00017-6

18. Wu, F.-C.; Tseng, R.-L.; Juang, R.-S.: A review and experimental verification of using chitosan and its derivatives as adsorbents for selected heavy metals. J. Environ. Manag. **91**, 798–806 (2010). https://doi.org/10.1016/j.jenvman.2009.10.018

19. Li, J.; Hu, J.; Sheng, G.; Zhao, G.; Huang, Q.: Effect of pH, ionic strength, foreign ions and temperature on the adsorption of Cu(II) from aqueous solution to GMZ bentonite. Colloids Surf. A Physicochem. Eng. Asp. **349**, 195–201 (2009). https://doi.org/10.1016/j.colsurfa.2009.08.018

20. Zahedifar, M.; Seyedi, N.; Salajeghe, M.; Shafiei, S.: Nanomagnetic biochar dots coated silver NPs (BCDs-Ag/MNPs): a highly efficient catalyst for reduction of organic dyes. Mater. Chem.

Phys. **246**, 122789 (2020). https://doi.org/10.1016/j.matchemphys.2020.122789

21. Jones, D.L.; Rousk, J.; Edwards-Jones, G.; DeLuca, T.H.; Murphy, D.V.: Biochar-mediated changes in soil quality and plant growth in a three year field trial. Soil Biol. Biochem. **45**, 113–124 (2012). https://doi.org/10.1016/j.soilbio.2011.10.012

22. Batista, E.M.C.C.; Shultz, J.; Matos, T.T.S.; Fornari, M.R.; Ferreira, T.M.; Szpoganicz, B.; de Freitas, R.A.; Mangrich, A.S.: Effect of surface and porosity of biochar on water holding capacity aiming indirectly at preservation of the Amazon biome. Sci. Rep. **8**, 1–9 (2018). https://doi.org/10.1038/s41598-018-28794-z

23. Jian, X.; Zhuang, X.; Li, B.; Xu, X.; Wei, Z.; Song, Y.; Jiang, E.: Comparison of characterization and adsorption of biochars produced from hydrothermal carbonization and pyrolysis. Environ. Technol. Innov. **10**, 27–35 (2018). https://doi.org/10.1016/j.eti.2018.01.004

24. Deem, L.M.; Crow, S.E.: Biochar. In: Reference Module in Earth Systems and Environmental Sciences. Elsevier, Amsterdam (2017)

25. Chatterjee, S.; Lim, S.-R.; Woo, S.H.: Removal of reactive black 5 by zero-valent iron modified with various surfactants. Chem. Eng. J. **160**, 27–32 (2010). https://doi.org/10.1016/j.cej.2010.02.045

26. Zhou, Y.; Gao, B.; Zimmerman, A.R.; Chen, H.; Zhang, M.; Cao, X.: Biochar-supported zerovalent iron for removal of various contaminants from aqueous solutions. Bioresour. Technol. **152**, 538–542 (2014). https://doi.org/10.1016/j.biortech.2013.11.021

27. Aklil, A.; Mouflih, M.; Sebti, S.: Removal of heavy metal ions from water by using calcined phosphate as a new adsorbent. J. Hazard. Mater. **112**, 183–190 (2004). https://doi.org/10.1016/j.jhazmat.2004.05.018

28. Watanabe, F.S.; Olsen, S.R.: Test of an ascorbic acid method for determining phosphorus in water and $NaHCO_3$ extracts from soil 1. Soil Sci. Soc. Am. J. **29**, 677–678 (1965). https://doi.org/10.2136/sssaj1965.03615995002900060025x

29. Johnson, K.S.; Petty, R.L.: Determination of phosphate in seawater by flow injection analysis with injection of reagent. Anal. Chem. **54**, 1185–1187 (1982). https://doi.org/10.1021/ac00244a039

30. Zahedifar, M.; Pouramiri, B.; Razavi, R.: Triethanolamine lactate-supported nanomagnetic cellulose: a green and efficient catalyst for the synthesis of pyrazolo[3,4-b]quinolines and theoretical study. Res. Chem. Intermed. **46**, 2749–2765 (2020). https://doi.org/10.1007/s11164-020-04117-8

31. Ahmad, M.; Usman, A.R.A.; Rafique, M.I.; Al-Wabel, M.I.: Engineered biochar composites with zeolite, silica, and nano-zerovalent iron for the efficient scavenging of chlortetracycline from aqueous solutions. Environ. Sci. Pollut. Res. **26**, 15136–15152 (2019). https://doi.org/10.1007/s11356-019-04850-7

32. Lin, Y.; Munroe, P.; Joseph, S.; Kimber, S.; Van Zwieten, L.: Nanoscale organo-mineral reactions of biochars in ferrosol: an investigation using microscopy. Plant Soil. **357**, 369–380 (2012). https://doi.org/10.1007/s11104-012-1169-8

33. Mohan, D.; Sarswat, A.; Ok, Y.S.; Pittman, C.U.: Organic and inorganic contaminants removal from water with biochar, a renewable, low cost and sustainable adsorbent—a critical review. Bioresour. Technol. **160**, 191–202 (2014). https://doi.org/10.1016/j.biortech.2014.01.120

34. Zhang, M.; Li, J.; Wang, Y.: Impact of biochar-supported zerovalent iron nanocomposite on the anaerobic digestion of sewage sludge. Environ. Sci. Pollut. Res. **26**, 10292–10305 (2019). https://doi.org/10.1007/s11356-019-04479-6

35. Yusuf, A.A.; Inambao, F.L.: Characterization of Ugandan biomass wastes as the potential candidates towards bioenergy production. Renew. Sustain. Energy Rev. **117**, 109477 (2020)

36. Ahmad, M.; Ahmad, M.; Usman, A.R.A.; Al-Faraj, A.S.; Abduljabbar, A.S.; Al-Wabel, M.I.: Biochar composites with nano

zerovalent iron and eggshell powder for nitrate removal from aqueous solution with coexisting chloride ions. Environ. Sci. Pollut. Res. **25**, 25757–25771 (2018). https://doi.org/10.1007/s11356-017-0125-9

37. Shi, L.; Zhang, X.; Chen, Z.: Removal of chromium (VI) from wastewater using bentonite-supported nanoscale zero-valent iron. Water Res. **45**, 886–892 (2011). https://doi.org/10.1016/j.watres.2010.09.025

38. Sun, Y.-P.; Li, X.; Cao, J.; Zhang, W.; Wang, H.P.: Characterization of zero-valent iron nanoparticles. Adv. Colloid Interface Sci. **120**, 47–56 (2006). https://doi.org/10.1016/j.cis.2006.03.001

39. Qian, L.; Zhang, W.; Yan, J.; Han, L.; Chen, Y.; Ouyang, D.; Chen, M.: Nanoscale zero-valent iron supported by biochars produced at different temperatures: synthesis mechanism and effect on Cr(VI) removal. Environ. Pollut. **223**, 153–160 (2017). https://doi.org/10.1016/j.envpol.2016.12.077

40. Singh, R.; Gautam, N.; Mishra, A.; Gupta, R.: Heavy metals and living systems: an overview. Indian J. Pharmacol. **43**, 246–253 (2011). https://doi.org/10.4103/0253-7613.81505

41. Chen, Y.-F.; Kao, C.-L.; Yang, J.-F.; Huang, P.-C.; Hsu, C.-Y.; Kuei, C.-H.: A Simple extraction method for determination of high molecular weight polycyclic aromatic hydrocarbons in sediments by gas chromatography–mass spectrometry. J. Chin. Chem. Soc. **62**, 766–771 (2015). https://doi.org/10.1002/jccs.201500184

42. Zhou, Y.; Liu, X.; Xiang, Y.; Wang, P.; Zhang, J.; Zhang, F.; Wei, J.; Luo, L.; Lei, M.; Tang, L.: Modification of biochar derived from sawdust and its application in removal of tetracycline and copper from aqueous solution: adsorption mechanism and modelling. Bioresour. Technol. **245**, 266–273 (2017). https://doi.org/10.1016/j.biortech.2017.08.178

43. Delgado, N.; Capparelli, A.; Navarro, A.; Marino, D.: Pharmaceutical emerging pollutants removal from water using powdered activated carbon: study of kinetics and adsorption equilibrium. J. Environ. Manag. **236**, 301–308 (2019). https://doi.org/10.1016/j.jenvman.2019.01.116

44. Mohapatra, R.K.; Parhi, P.K.; Pandey, S.; Bindhani, B.K.; Thatoi, H.; Panda, C.R.: Active and passive biosorption of Pb(II)using live and dead biomass of marine bacterium *Bacillus xiamenensis* PbRPSD202: kinetics and isotherm studies. J. Environ. Manag. **247**, 121–134 (2019). https://doi.org/10.1016/j.jenvman.2019.06.073

45. Lal Homagai, P.; Ghimire, K.N.; Inoue, K.: Adsorption behavior of heavy metals onto chemically modified sugarcane bagasse. Bioresour. Technol. **101**, 2067–2069 (2010). https://doi.org/10.1016/j.biortech.2009.11.073

46. Shen, W.; Chen, S.; Shi, S.; Li, X.; Zhang, X.; Hu, W.; Wang, H.: Adsorption of Cu(II) and Pb(II) onto diethylenetriamine-bacterial cellulose. Carbohydr. Polym. **75**, 110–114 (2009). https://doi.org/10.1016/j.carbpol.2008.07.006

47. Zhu, S.; Ho, S.-H.; Huang, X.; Wang, D.; Yang, F.; Wang, L.; Wang, C.; Cao, X.; Ma, F.: Magnetic nanoscale zerovalent iron assisted biochar: interfacial chemical behaviors and heavy metals remediation performance. ACS Sustain. Chem. Eng. **5**, 9673–9682 (2017). https://doi.org/10.1021/acssuschemeng.7b00542

48. Naowanat, N.; Thouchprasitchai, N.; Pongstabodee, S.: Adsorption of emulsified oil from metalworking fluid on activated bleaching earth-chitosan-SDS composites: optimization, kinetics, isotherms. J. Environ. Manag. **169**, 103–115 (2016). https://doi.org/10.1016/j.jenvman.2015.12.024

49. Wang, H.; Gao, B.; Wang, S.; Fang, J.; Xue, Y.; Yang, K.: Removal of Pb(II), Cu(II), and Cd(II) from aqueous solutions by biochar derived from $KMnO_4$ treated hickory wood. Bioresour. Technol. **197**, 356–362 (2015). https://doi.org/10.1016/j.biortech.2015.08.132

50. Inyang, M.; Gao, B.; Yao, Y.; Xue, Y.; Zimmerman, A.R.; Pullammanappallil, P.; Cao, X.: Removal of heavy metals from aqueous solution by biochars derived from anaerobically digested biomass. Bioresour. Technol. **110**, 50–56 (2012). https://doi.org/10.1016/j.biortech.2012.01.072